# The retina uncouples glycolysis and oxidative phosphorylation via Cori-, Cahill-, and mini-Krebs-cycle

Yiyi Chen[1, 5], Laimdota Zizmare[2, 5], Victor Calbiague[3], Lan Wang[1], Shirley Yu[1], Friedrich W. Herberg[4], Oliver Schmachtenberg[3], François Paquet-Durand[1, 5, 6*], Christoph Trautwein[2, 5*]

[1] Institute for Ophthalmic Research, University of Tübingen, 72076, Germany

[2] Werner Siemens Imaging Center, Department of Preclinical Imaging and Radiopharmacy, University of Tübingen, 72076, Germany

[3] Centro Interdisciplinario de Neurociencia de Valparaíso, Universidad de Valparaíso, Chile

[4] Biochemistry Department, University of Kassel, 34132, Germany

[5] These authors contributed equally

[6] Lead contact

* Corresponding authors: François Paquet-Durand, Christoph Trautwein.

**Email:** francois.paquet-durand@klinikum.uni-tuebingen.de
christoph.trautwein@med.uni-tuebingen.de

## Highlights

- The retina utilizes a complex energy switchboard consisting of the Krebs cycle, mini-Krebs cycle, Cahill cycle, and Cori cycle.
- Mini-Krebs cycle runs more efficiently than 'full' Krebs cycle.
- Alanine transaminase decouples glycolysis from the Krebs cycle.
- Lactate, alanine, and N-acetylaspartate are distinctive energetic pathway signatures.

## Abstract

The retina consumes massive amounts of energy, yet its metabolism and substrate exploitation remain poorly understood. Here, we used a murine explant model to manipulate retinal energy metabolism under entirely controlled conditions and utilized $^{1}$H-NMR spectroscopy-based metabolomics, *in situ* enzyme detection, and cell viability readouts to uncover the pathways of retinal energy production. Our experimental manipulations resulted in varying degrees of photoreceptor degeneration, while the inner retina and retinal pigment epithelium were essentially unaffected. This selective vulnerability of photoreceptors suggested very specific adaptations in their energy metabolism. Rod photoreceptors were found to rely strongly on oxidative phosphorylation, but only mildly on glycolysis. Conversely, cone photoreceptors were highly dependent on glycolysis but insensitive to electron transport chain decoupling. Importantly, photoreceptors were able to uncouple glycolytic and Krebs-cycle metabolism via three different pathways: 1) the mini-Krebs-cycle, fueled by glutamine and branched-chain amino acids, generating N-acetylaspartate; 2) the alanine-generating Cahill-cycle; 3) the lactate-releasing Cori-cycle. Moreover, the metabolomic data indicated a shuttling of taurine and hypotaurine between the retinal pigment epithelium and photoreceptors, resulting in an additional net transfer of reducing power to photoreceptors. These findings expand our understanding of retinal physiology and pathology and shed new light on neuronal energy homeostasis and the pathogenesis of neurodegenerative diseases.

## Keywords

Energy homeostasis, glucose transport, aerobic glycolysis, glucose-alanine cycle, alanine transaminase, aspartate amino transferase

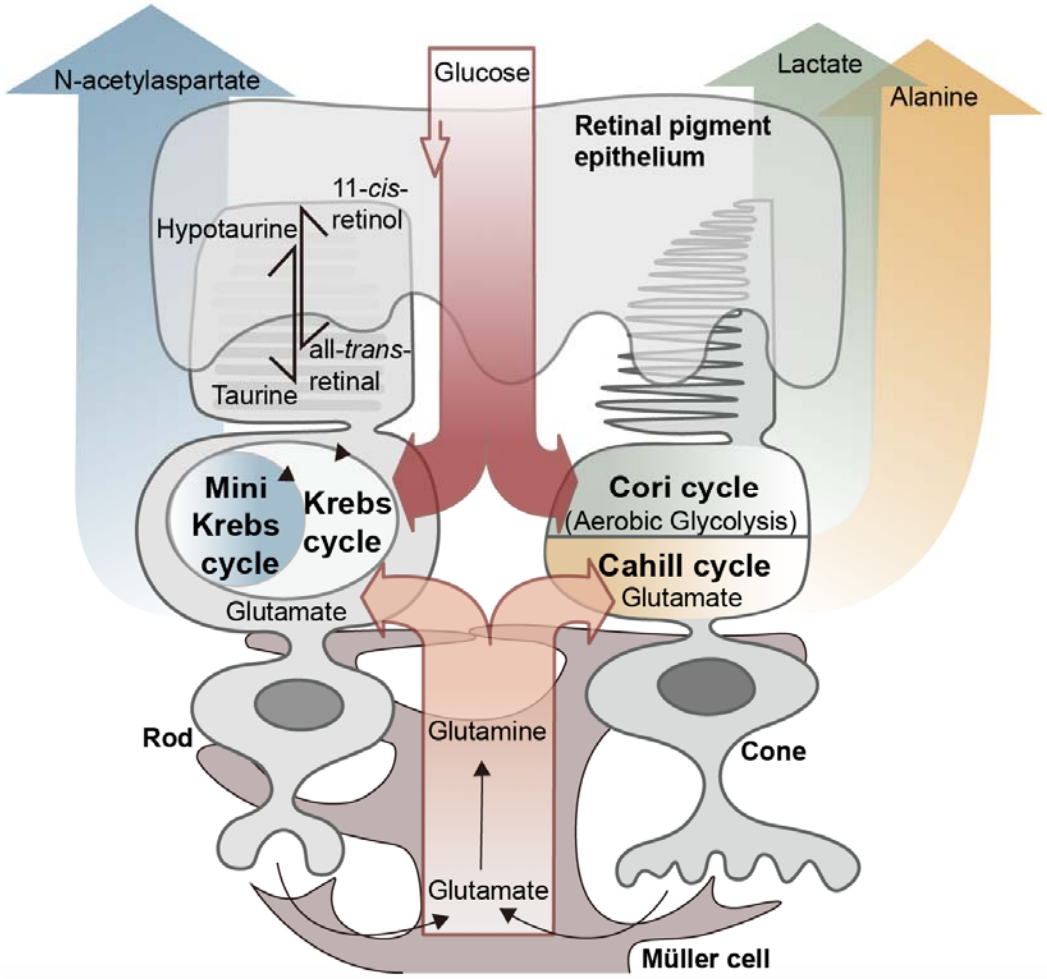


**Graphical abstract**: Retinal photoreceptors employ both glucose and glutamate as fuels. While rod photoreceptors rely strongly on oxidative phosphorylation and the N-acetylaspartate producing mini-Krebs-cycle, cone photoreceptors rely on the lactate-producing Cori cycle and the oxidative, alanine-producing Cahill cycle.

**Abbreviations**

1,9-DDF – 1,9 dideoxyforskolin, AA – amino acids, AAT – aspartate amino transferase, ADP – adenosine diphosphate, ALT – alanine transaminase, ATP – adenosine triphosphate, BCAA – branched chain amino acid, COX – cytochrome oxidase, GAC – glutaminase C, GCs – ganglion cells, GLUT - glucose transporter, GS – glutamine synthase, GTP – guanosine triphosphate, GABA – gamma amino butyric acid, GPC – sn-glycero-3-phosphate, FCCP – carbonyl cyanide-*p*-trifluoromethoxyphenylhydrazone, GSSG – glutathione disulfide, INL – inner nuclear layer, MGC – Müller glial cells, NAA – N-acetylaspartate, $NAD^+$ – nicotinamide adenine dinucleotide, ONL – outer nuclear layer, O-PE – O-phosphoethanolamine, OXPHOS – oxidative phosphorylation, PARP – poly(ADP)ribose polymerase, PCK – phosphoenolpyruvate carboxy kinase, PKM – pyruvate kinase M, PNA - peanut agglutinin, RP – retinitis pigmentosa, RPE – retinal pigment epithelium, RPE65 – retinal pigment epithelium-specific 65 kDa protein, SUCLG1 – succinate-CoA ligase-1, TUNEL – terminal UDP nick-end labelling, UDP – uracil diphosphate

## Introduction

The retina is the neuronal tissue with the highest energy demand (1, 2). Paradoxically, the mammalian retina is thought to strongly rely on energy-inefficient glycolysis, even though oxygen is available and high-yield oxidative phosphorylation (OXPHOS) possible (3). This aerobic glycolysis releases large amounts of lactate, as already reported in the 1920s by Otto Warburg (4). High retinal energy demand is linked to the extraordinary single-photon sensitivity of photoreceptors (2, 5, 6), and to lipid synthesis for the constant renewal of photoreceptor outer segments (7, 8).

The retina harbors two types of photoreceptors: rods, which exhibit remarkable light sensitivity and enable night vision; and cones, which work in daylight and allow color vision. Cones spend around twice as much energy as rods (9). Photoreceptors are not connected to the vasculature and are nourished by other retinal cell types, including retinal pigment epithelial (10) cells or Müller glial cells (MGC). Moreover, photoreceptors can experience changes in energy demand on a millisecond timescale, from very high in the dark, to 4-10 times lower in light (5).

Glycolysis provides for rapid but inefficient adenosine triphosphate (ATP) production, while Krebs-cycle and OXPHOS are very efficient but much slower. Since glycolysis and Krebs-cycle are metabolically coupled through pyruvate, it is unclear how photoreceptors adapt to sudden and large changes in energy demand, and what energy substrates they may use. A recent hypothesis proposed that photoreceptors use predominantly aerobic glycolysis, with the resultant lactate utilized by the retinal pigment epithelium (RPE) and MGCs for OXPHOS (11). However, this contrasts with the high density of mitochondria in photoreceptor inner segments. Retinal energy metabolism has obvious ramifications for disease pathogenesis, including diabetic retinopathy, age-related macular degeneration, or inherited retinal diseases, such as retinitis pigmentosa.

Here, we studied expression of energy metabolism-related enzymes in different retinal cell types, using organotypic retinal explants maintained in serum-free, fully defined medium. Metabolic functions of the RPE were investigated by culturing retina with and without RPE. As readouts, we correlated enzyme expression with quantitative proton nuclear magnetic resonance ($^{1}$H-NMR) spectroscopy-based metabolomics and cell death. Notably, interventions in energy metabolism caused selective photoreceptor cell death, while leaving other retinal cell types unaffected. Metabolomic analysis and localization of key enzymes identified important pathways and shuttles altered, explaining the strong interdependence of the various retinal cell types, and opening new perspectives for the treatment of neurodegenerative diseases in the retina and beyond.

## Results

### Retinal expression patterns of key energy metabolism related enzymes

We used immunofluorescence to assess expression and cellular localization of enzymes important for retinal metabolism (Figure 1). The outermost retinal layer is formed by RPE cells expressing RPE-specific 65kDa protein (RPE65), dedicated to the recycling of photopigment retinal (12). Hence, RPE65 immunolabeling revealed the RPE cell monolayer (Figure 1A). Immunofluorescence for glucose-transporter-1 (GLUT1) showed strong labelling on basal and apical sides of RPE cells (Figure 1A), in line with previous literature (3, 13). Glucose uptake from the RPE into the neuroretina is mediated by high affinity/high capacity GLUT3 (14), strongly expressed on photoreceptor inner segments (Supplementary Figure 1A). Pyruvate kinase is essential to glycolysis, catalyzing the conversion of phosphoenolpyruvate to pyruvate. While pyruvate kinase M1 (PKM1) was expressed in the inner retina (Supplementary Figure 1A), PKM2 was found in photoreceptor inner segments and synapses (Figure 1A). Expression of mitochondrial cytochrome oxidase (COX) largely overlapped with PKM2 (Figure 1A).

106

107 **Challenging energy metabolism reduces rod and cone photoreceptor viability**

108 To dissect retinal energy metabolism, we selectively manipulated key pathways (Figure 1B) using
109 organotypic retinal explants (17) (Supplementary Figure 1B). Retinal cultures were prepared with the RPE
110 cell layer attached to the neuroretina (control) or without RPE (*no* RPE). The *in vivo* expression patterns of
111 enzymes important for energy metabolism (Figure 1A) were comparable in the *in vitro* situation
112 (Supplementary Figure 1C). In control, the rate of cell death in the outer nuclear layer (ONL), as assessed
113 by the TUNEL assay (Figure 1C, D), was low (0.46%±0.22, n=9). The *no* RPE condition displayed significantly
114 increased photoreceptor cell death (3.35%±1.62, n=5, p<0.001). Blocking RPE glucose transport with the
115 selective GLUT1 inhibitor 1,9-dideoxyforskolin (1,9-DDF) (18) further increased ONL cell death
116 (6.77%±1.57, n=5, p<0.0001). The inhibition of glycolytic PKM2 with Shikonin (19), and OXPHOS disruption
117 with the electron chain uncoupler carbonyl cyanide-p-trifluoromethoxyphenylhydrazone (FCCP) (16) both
118 caused a significant increase in photoreceptor cell death (Shikonin: 17.75%±2.13, n=5, p<0.0001; FCCP:
119 22.49 % ± 6.79, n=5, p<0.0001). All four experimental interventions mostly affected photoreceptors, not
120 significantly reducing the viability of other retinal cell types (Figure 1C).

121 Remarkably, a differential effect on cone photoreceptor survival (Figure 1E, F) was observed as assessed
122 by immunodetection of the cone-specific marker arrestin-3 (Arr3). Control retina harbored 11.47 (±1.95,
123 n=9) cones per 100 µm of retinal circumference. noRPE retina displayed a significant decrease in cone
124 survival (4.62±1.39, n=5, p<0.0001), while blocking RPE glucose transport with 1,9-DDF led to an even
125 more dramatic reduction (1.02±1.09, n=5, p<0.0001). By comparison, inhibition of glycolysis with Shikonin
126 had a relatively mild effect on cone survival (7.78±1.36, n=5, p<0.0001). Surprisingly, FCCP treatment did
127 not cause cone death (12.84±1.75, n=5, p=0.22), compared to control.

128 We further calculated the percentages of dying cones and rods, assuming that 3% of all photoreceptors
129 were cones (20, 21) (Figure 1G, H). In the four treatment situations the ratios of cone to rod death were:
130 *no* RPE = 1:1; 1,9-DDF = 1:1.5; Shikonin = 1:17; and FCCP = 0: ∞. Cones were almost entirely depleted by
131 the 1,9-DDF treatment but remained virtually unaffected by the FCCP treatment. Rods, however, were
132 strongly and highly selectively affected by Shikonin and FCCP, while the *no* RPE condition had a relatively
133 minor effect. These results highlight important differences between rod and cone energy metabolism.

134

135 **Experimental retinal interventions produce characteristic metabolomic patterns**

136 We employed high-field (600 MHz) $^{1}$H-NMR spectroscopy-based metabolomics to study the metabolic
137 signatures in five experimental groups (Supplementary Table 1). A principal component analysis (PCA)
138 showed clear group separation (Figure 1I). Unbiased clustering of metabolite profiles revealed specific
139 groups that were differentiated among the five experimental situations (Figure 2A). The greatest cluster
140 overlap was seen in control and Shikonin groups. Significant clustering was observed in several amino acid
141 sub-classes and energy metabolites. We found the strongest changes in the 1,9-DDF condition, where
142 glutamate, aspartate, alanine, O-phosphocholine, and nicotinamide adenine dinucleotide ($NAD^{+}$)
143 concentrations were particularly upregulated compared to control. Further, branched-chain amino acids
144 (BCAAs), lactate, and threonine were upregulated in the FCCP and *no* RPE condition. Glutathione (GSH)
145 and glutathione disulfide (GSSG) were relatively reduced by Shikonin treatment, with increased creatine
146 and formate. Control and 1,9-DDF treatment displayed high levels of guanosine triphosphate (GTP),
147 adenosine triphosphate (ATP), and π-methylhistidine, which were low in the other groups (Figure 2A).

148 We then compared metabolite patterns for each treatment to control (Figure 2B). Metabolites were
149 grouped according to class and function, including fundamental metabolic pathways, such as energy and
150 cofactor metabolism, coenzymes, Krebs-cycle, neuronal tissue-associated metabolites and
151 neurotransmitters, BCAAs, glucogenic and ketogenic amino acids (AAs), serine synthesis pathway, cell
152 membrane synthesis, and individual features from redox metabolism. Afterward, the metabolomic

differences identified were explored in detail and related to the retinal expression of corresponding enzymes.

**Retina cultured without RPE displays strongly increased glycolytic activity**

The RPE is tightly bound to the choroid and serves as interface between vasculature and neuroretina. Because of the strong adherence of RPE to the choroid, most prior studies on explanted retina were performed without RPE (4, 11). To understand the metabolic communication between neuroretina and RPE, we prepared organotypic retinal explants both with RPE (control) or without RPE (*no* RPE).

The metabolite profile of control was markedly different from retina cultured without RPE, with 25 metabolites exhibiting significant changes (Figure 3A, Supplementary Figure 3). Decreased ATP levels in the *no* RPE group, corresponded to increased lactate. The BCAAs isoleucine, leucine, and valine, and some of the glucogenic/ketogenic AAs threonine, methionine, glycine, displayed higher levels in the *no* RPE group compared to control. Alanine, aspartate, and taurine showed the opposite trend. Hypotaurine, 4-aminobutyrate (GABA), and glutamate were accumulated in retinal tissue, while membrane synthesis-associated metabolites, such as myo-inositol and O-phosphocholine, as well as creatine and N-acetylaspartate (NAA) were reduced in neuroretina. Moreover, higher levels of GSSG appeared in the absence of RPE, pointing towards an altered redox metabolism.

Pattern hunter (Pearson R) correlation analysis found citrate, a central Krebs-cycle metabolite, positively correlated with taurine, alanine, aspartate, and ATP (Figure 3B). Negative correlations with citrate included ADP, BCAAs, and lactate. A subsequent KEGG-based pathway analysis revealed changes in arginine and proline metabolism, taurine and hypotaurine metabolism, and alanine, aspartate, and glutamate metabolism in the *no* RPE situation (Figure 3C).

Immunofluorescence was used to localize enzymes likely responsible for the observed metabolic changes (Figure 3D). Citrate synthase (CS) and fumarase, key enzymes of the Krebs-cycle, were found mostly in photoreceptor inner segments and synaptic terminals. The γ-subunit of ATP synthase, essential for OXPHOS, was also localized to photoreceptor inner segments and synapses. Thus, low ATP levels in the *no* RPE group likely resulted from decreased photoreceptor Krebs-cycle and OXPHOS activity. High levels of taurine were detected in photoreceptor inner segments and synapses, as well as in the ganglion cell layer (Figure 3D). Finally, the enzyme alanine transaminase (ALT), previously thought to be expressed only in muscle and liver, was found to be expressed in the inner nuclear and plexiform layers (Figure 3D). ALT was also strongly expressed in cone inner segments, as evidenced by co-labelling with cone -Arr3. This expression pattern and high alanine levels in the control strongly suggested Cahill-cycle activity in the retina (22). When ALT activity was inhibited with β-chloro-alanine, photoreceptor cell death was increased and notably cone survival was reduced, validating the functional expression of ALT in the outer retina (Supplementary Figure 4A, B).

The patterns observed in the *no* RPE to control comparison indicated that retinal metabolism strongly depends on RPE-to-neuroretina interactions, including shuttling of metabolites such as hypotaurine/taurine. Notably, the accumulation of BCAA, glutamate, and lactate, concomitant with decreased alanine levels in the *no* RPE group, implied that RPE removal switched retinal metabolism from Krebs-cycle/OXPHOS to aerobic glycolysis.

**Photoreceptors use the Krebs-cycle to produce GTP**

We further compared metabolite patterns between *no* RPE and FCCP groups. In Figure 2, the *no* RPE and FCCP groups showed similar metabolite patterns and pathway changes overall. However, a detailed statistical analysis revealed 17 significant metabolite changes (Figure 4A; Supplementary Figure 5). Among the most highly reduced metabolite concentrations in the FCCP group was GTP, which positively

199 correlated with GABA, ATP, GSSG, hypotaurine, and $NAD^+$ (Figure 4B). In contrast, GDP, BCAAs, glutamine,
200 and citrate negatively correlated to GTP. The KEGG-based pathway analysis ranked glycine, serine and
201 threonine metabolism, glutathione metabolism, and alanine, aspartate and glutamate metabolism as the
202 most significantly changed between the two conditions (Figure 4C).

203 Curiously, measurable amounts of GTP can only be generated in two ways: 1) by succinate-CoA ligase,
204 GTP-forming-1 (SUCLG-1) in the Krebs-cycle, and 2) by nucleoside-diphosphate kinase (NDK) from excess
205 ATP. Since ATP levels were low in both the FCCP and the no RPE situation, here, GTP could not have been
206 produced from ATP. Immunofluorescence for SUCLG-1 showed strong expression in photoreceptor inner
207 segments and synapses, where it co-localized to a large extent with mitochondrial COX (Figure 4D).
208 Hence, the SUCLG-1 retinal expression pattern and the synthesis of GTP in the absence of RPE provided
209 clear evidence for Krebs-cycle activity in photoreceptors.

210 We also identified an FCCP-induced upregulation of citrate, concomitant with a downregulation of $NAD^+$.
211 This indicated a Krebs-cycle interruption at the level of D-isocitrate to α-ketoglutarate conversion, *i.e.*, a
212 step that requires $NAD^+$. $NAD^+$ is known to be consumed by poly-ADP-ribose-polymerase (PARP), which is
213 activated by oxidative DNA damage (23) and up-regulated in dying photoreceptors (24). Therefore, we
214 quantified poly-ADP-ribose (PAR) accumulation in retinal cells as a marker for PARP activity. Compared to
215 the *no* RPE group, more photoreceptor cells in the FCCP-treated retina showed PAR accumulation,
216 correlating with decreased retinal $NAD^+$ levels (Figure 4E, F). Hence, FCCP-induced oxidative stress may
217 cause increased PARP activity and decreased $NAD^+$ levels, eventually interrupting the Krebs-cycle, as
218 evidenced by citrate accumulation.

219 Overall, the data from the *no* RPE to FCCP group comparison showed that disruption of OXPHOS led to AA
220 accumulation, including lysine, phenylalanine, glutamine, leucine, and valine. Notably, alanine
221 accumulation in the FCCP group was likely caused by ALT-dependent pyruvate transamination. By
222 contrast, metabolites high in the *no RPE* group but low with FCCP treatment were probably generated via
223 the Krebs-cycle in the neuroretina. This concerned especially GTP, aspartate, and NAA.

224

225 **Reduced retinal glucose uptake promotes anaplerotic metabolism**

226 Since GLUT1 was predominantly expressed in the RPE, we initially assumed that the metabolic response
227 to 1,9-DDF treatment might resemble that of the *no* RPE situation. However, the patterns found between
228 these two groups were very different (*cf.* Figure 2) revealing 28 significantly changed metabolites (Figure
229 5A; Supplementary Figure 6). When compared to the *no* RPE, the 1,9-DDF group showed changes in
230 mitochondria and Krebs-cycle-associated metabolites (*e.g.*, high ATP, high formate, low BCAA).
231 Conversely, the Cahill-cycle product alanine and NAA were upregulated by 1,9-DDF treatment. The
232 pattern hunter analysis showed that metabolites formate, glutamate, taurine, and citrate were positively
233 correlated with ATP, while, AMP, GMP, and BCAA were negatively correlated with ATP (Figure 5B).

234 The KEGG pathway analysis showed alanine, aspartate, and glutamate metabolism, glutathione
235 metabolism and glycine, serine, and threonine metabolism among the three most affected pathways
236 (Supplementary Figure 6B). Taken together, the depletion of BCAAs in the 1,9-DDF treatment indicated
237 that the retina used anaplerotic substrates to fuel the Krebs-cycle and maintain ATP production.

238

239 **Inhibition of glycolysis strongly impacts retinal ATP production**

240 We compared the Shikonin treatment, which inhibits the last step of glycolysis, to the FCCP treatment,
241 which abolishes mitochondrial ATP synthesis (Figure 5C). Formate, aspartate, and NAA were increased in
242 the Shikonin group. Conversely, higher amounts of GSH, GSSG, BCAA, threonine, and phenylalanine after
243 FCCP treatment indicated Krebs-cycle interruption (Supplementary Figure 7). The production of lactate
244 was higher with FCCP- compared to Shikonin treatment, reflecting increased glycolysis to compensate for

245 the loss of Krebs-cycle-dependent ATP production. Metabolites connected to oxidative stress, such as
246 GSSG and GSH, were also increased by FCCP treatment. Pattern hunter for metabolites correlated with
247 glutathione found 3-hydroxyisovalerate, glutamine, GSSG, but also lactate and ATP, while succinate,
248 alanine, and GABA were negatively correlated with GSH (Figure 5D). The subsequent pathway analysis
249 identified arginine biosynthesis, alanine, aspartate, and glutamate metabolism, as well as glycolysis and
250 gluconeogenesis as the most strongly regulated metabolic pathways (Supplementary Figure 7B).

251

252 **Blocking glucose uptake and OXPHOS uncoupling reveal distinct rod and cone metabolism**

253 The metabolic rate of cones is at least two times higher than that of rods (9). The treatment with 1,9-DDF
254 resulted in near complete cone loss, while cones were fully preserved with FCCP treatment (*cf.* Figure 1).
255 Therefore, we compared these two experimental groups with control to investigate the relative
256 contributions of rods and cones to the metabolite patterns observed.

257 In this three-way comparison, 29 metabolite concentrations were significantly changed (Figure 6A;
258 Supplementary Figure 8). The FCCP treatment reduced ATP and GTP levels, while lactate production was
259 greatly increased, along with methionine and threonine. BCAAs, glutamine, phenylalanine and tyrosine
260 also showed a significant upregulation with FCCP treatment. Interestingly, some metabolites like GSSG,
261 serine, glutamate, alanine, $NAD^+$, and taurine displayed a pronounced increase in the 1,9-DDF group when
262 compared to either control or FCCP. In addition, formate, aspartate, and myo-inositol were upregulated
263 with 1,9-DDF treatment, together with NAA and creatine. Finally, the comparison between the 1,9-DDF
264 and FCCP groups revealed highly increased levels of ATP and GTP, implying a strong activation of the
265 Krebs-cycle under 1,9-DDF treatment.

266 A cell type-specific attribution of these metabolite patterns may be superseded by direct drug treatment
267 effects. Using only metabolite changes in opposing directions from control to interpret different cellular
268 compositions, we identified BCAAs, tyrosine, NAA, and ATP (Supplementary Figure 8). BCAAs and tyrosine
269 (and glutamine) exhibited low levels in the rod-rich 1,9-DDF group and high levels in the cone-rich FCCP
270 group, indicating that these metabolites might be consumed by rods or produced in cones. Vice versa, it
271 can be assumed that aspartate and NAA were predominantly produced in rods.

272 To investigate the role of glutamine in retinal metabolism, we used immunofluorescence (Figure 6B). We
273 confirmed a strong expression of glutamine synthase (GS) in MGCs (25). Remarkably, the enzyme that
274 hydrolyses glutamine to glutamate, glutaminase C (GAC) was prominently expressed in photoreceptor
275 inner segments, photoreceptor synapses, and INL. Co-labelling with cone Arr3 revealed a strong
276 expression of GAC in cone inner segments, implying that cones use glutamine imported from MGCs as a
277 metabolic substrate. Accordingly, treatment with the GAC-specific inhibitor Compound 968 dose-
278 dependently reduced photoreceptor viability, while leaving the inner retina mostly intact (Supplementary
279 Figure 4C, D).

280

281 **Impact on glycolytic activity, serine synthesis pathway, and anaplerotic metabolism**

282 To assess how the various experimental interventions affected retinal metabolism, we calculated the
283 ratios for pathway-specific metabolites (Figure 6C). GTP, when produced by SUCLG-1, is a marker for
284 Krebs-cycle activity, while lactate indicates glycolytic activity. In the *no* RPE group, the GTP-to-lactate ratio
285 was significantly lower than in control, indicating 4.1-times higher glycolytic activity. While in the 1,9-DDF
286 and Shikonin group the GTP-to-lactate ratios were not significantly different from control, with FCCP
287 treatment this ratio dropped to the lowest level, in line with a strong downregulation of Krebs-cycle and
288 concomitant upregulation of glycolysis.

289 We then calculated the ratio of serine to lactate as an indicator for serine synthesis pathway activity.
290 Under control conditions, and in the *no* RPE and FCCP groups, this activity was rather low, while it was

291 strongly increased by 1,9-DDF and Shikonin treatment. In the Shikonin group, serine production from 3-
292 phosphoglycerate and subsequent deamination to pyruvate may bypass the PKM2 block. Serine is also a
293 precursor of phosphatidylserine, one of the three main cell membrane components. Together with a
294 reduction of choline and high concentrations of myo-inositol, O-phosphocholine, and O-
295 phosphoethanolamine, this may reflect high cell membrane synthesis under 1,9-DDF treatment.

296 Finally, we used the ratio of GTP to BCAAs to investigate to what extent Krebs-cycle activity was driven by
297 anaplerotic metabolism. A comparatively low GTP to BCAA ratio in the *no* RPE situation showed that much
298 of the GTP generated in the neuroretina likely came from anaplerotic substrates. While both Shikonin and
299 FCCP treatment decreased BCAA use, 1,9-DDF treatment increased anaplerotic metabolism.

300

301 **Evidence for mini-Krebs-cycle activity**

302 Comparing the ratios of GTP to lactate with GTP to BCAA in the *no* RPE situation showed that a large
303 proportion of the GTP produced in the neuroretina by SUCLG-1 was derived from anaplerotic substrates
304 rather than from pyruvate. These substrates enter the Krebs-cycle mostly at the level of α-ketoglutarate,
305 suggesting that the neuro-retinal Krebs-cycle might not start with citrate. Instead, only an α-ketoglutarate
306 to oxaloacetate shunt would be employed, including the GTP-synthesizing step from succinyl-CoA to
307 succinate (Figure 7A). A key step of this mini-Krebs-cycle (28) is the transamination of oxaloacetate with
308 glutamate by aspartate aminotransferase (AAT) to yield α-ketoglutarate and aspartate, which is further
309 acetylated to NAA. To investigate this possibility, we analyzed eight metabolites associated with the
310 Krebs-cycle (citrate, succinate, fumarate, GTP) and hypothesized mini-Krebs-cycles (glutamine, glutamate,
311 aspartate, NAA).

312 Hierarchical clustering showed similar patterns for aspartate and NAA in all experimental conditions
313 (Figure 7B). Except for the FCCP treatment, the ratio of citrate/NAA was 0.5, indicating that the retina
314 preferred the mini-Krebs-cycle over the full Krebs-cycle (Figure 7C). Immunolabelling for AAT –
315 conventionally associated with muscle and liver metabolism (29, 30) – found both AAT1 and AAT2 to be
316 expressed in photoreceptor inner segments and cell bodies (Figure 7D). This confirmed that
317 photoreceptors can execute the mini-Krebs-cycle, while the NAA production seen in the metabolomic
318 data demonstrated that this cycle was indeed used.

319 Finally, we compared the energetic efficiencies of glycolysis, Krebs, Cori, Cahill, and mini-Krebs cycle
320 (Figure 8). Using anaplerotic substrates the Cahill and mini-Krebs cycle allows for far more efficient energy
321 production compared to the Cori-cycle. Moreover, mitochondrial PCK2 can regenerate pyruvate from
322 oxaloacetate. Assuming that one mole of NADH/$FADH_2$ can be used to generate three moles of ATP via
323 OXPHOS, and depending on the exact stoichiometry of glutamate/BCAA input, the mini-Krebs-cycle may
324 deliver up to 18 moles of ATP and 2 moles of GTP per 3 carbon unit. Astonishingly, this exceeds the 15
325 moles of ATP and 1 mole of GTP generated in the "full" Krebs-cycle.

326

## 327 Discussion

328 This study combined cellular enzyme expression patterns with quantitative metabolomics of retinal
329 explants. In an entirely controlled environment, this enabled a comprehensive assessment of retinal
330 metabolism and allowed to analyze the impact of different experimental conditions upon cell death and
331 survival of retinal cells. As opposed to earlier works, our study highlights the crucial importance of
332 OXPHOS and anaplerotic pathways for the maintenance and survival of rod and cone photoreceptors.
333 Importantly, we show that photoreceptors can uncouple glycolysis and Krebs-cycle using a NAA-producing
334 shunt, allowing optimal function of both pathways and solving a long-standing problem in neuronal
335 energy metabolism research. Because of the ramifications for overall cellular physiology, these findings

are highly relevant for future therapy developments, for retinal diseases, as well as for neurodegenerative and further metabolic diseases in general.

**Photoreceptors use glucose and anaplerotic substrates as fuel**

Under anaerobic conditions, the production of lactate from glucose is a hallmark of skeletal muscle function. Here, pyruvate is reduced to lactate, which enters the bloodstream to serve as substrate for liver gluconeogenesis. Glucose can then cycle back to the muscle. This glucose-lactate cycle between muscle and liver was discovered in the 1930s and is referred to as Cori-cycle (32). The release of large amounts of lactate from isolated retina suggested that also the retina might use the Cori-cycle, albeit under aerobic conditions (33). Photoreceptors have thus been proposed to consume primarily glucose via aerobic glycolysis (11). The resultant lactate would be used as fuel in the Krebs-cycle by RPE and MGCs, generating ATP via OXPHOS. However, this hypothesis is contradicted by the high density of mitochondria in photoreceptor inner segments (26). Moreover, key enzymes for Krebs-cycle (CS, FH, SUCLG1) and OXPHOS (COX, ATP synthase γ) were strongly expressed in photoreceptors, but showed little or no expression in RPE or MGCs, in line with previous research (34). When we cultured retina without RPE, as done by Warburg and others (4, 11), we confirmed a strong lactate production. Yet, in retina cultured with RPE, lactate production was minor. Moreover, retina without RPE still produced large amounts of GTP, likely stemming from SUCLG1 activity and demonstrating Krebs-cycle operation in photoreceptors. Neuroretina without RPE displayed reduced viability of both rod and cone photoreceptors, as well as an accumulation of BCAAs and lactate. In contrast, the block of glucose import into the RPE by treatment with 1,9-DDF (18) resulted in a depletion of BCAAs and other AAs, and an increase of retinal ATP, demonstrating a switch from glycolytic to anaplerotic metabolism (28). Hence, we show that photoreceptors consume both glucose and anaplerotic substrates as fuels, and that retinal metabolism switches to aerobic glycolysis only in the absence of RPE. This switch is likely driven by increased glucose uptake. Normally, tight junction-coupled RPE cells form the outer blood-retinal barrier and prevent direct access of glucose to photoreceptors (35). In the absence of RPE, photoreceptors expressing the high affinity/high capacity GLUT3 become "flooded" with glucose. The resultant Crabtree effect then causes a shutdown of Krebs-cycle activity (14, 36, 37). Taken together, the high rates of retinal aerobic glycolysis first reported by Otto Warburg are likely an artefact of the absence of RPE, while intact retina may rely more on OXPHOS for its energy production.

**Rods need OXPHOS, cones need glycolysis**

Treatment with FCCP revealed striking differences between rod and cone energy metabolism. FCCP eliminates the proton gradient between inner mitochondrial membrane and mitochondrial matrix, abolishing ATP synthesis (16). Initially, FCCP may increase Krebs-cycle activity to attempt restoration of mitochondrial proton gradient (38), increasing oxidative stress (39) and oxidative DNA damage. The resultant activation of PARP would deplete $NAD^+$, further aggravating metabolic stress (40). Although FCCP had a strong toxic effect on rod photoreceptors, remarkably, cone photoreceptors were almost completely preserved. In striking contrast to the FCCP effect was that of the 1,9-DDF block on GLUT1(18). Although GLUT1 was strongly expressed in the RPE, glucose entering the RPE is shuttled forward to photoreceptors (10). Remarkably, with 1,9-DDF, over 90 % of cones were lost, while the detrimental effect on rods was comparatively minor. These differential effects of FCCP and 1,9-DDF strongly suggest that glycolysis is sufficient and necessary for cone survival, in agreement with earlier studies (41, 42). Conversely, rods require OXPHOS for their survival, while glycolysis is of minor importance. Furthermore, cone viability relative to rods was also strongly compromised in the *no* RPE situation, indicating that an intact blood-retinal barrier (35) and regulation of glucose access was important for cone survival. We note that GLUT2 may also contribute to photoreceptor glucose uptake (43).

383

384 **Cone photoreceptors use the Cahill-cycle**

385 The lactate-generating Cori-cycle (32) is highly inefficient and in intact retina likely plays a lesser role. An
386 efficient pathway is the glucose-alanine cycle, or Cahill-cycle, in which pyruvate, instead of being reduced
387 to lactate, is transaminated to alanine (22). This preserves NADH and generates α-keto acids to fuel the
388 Krebs-cycle. The alanine generated enters the bloodstream and is taken up by the liver, where the
389 ammonia is excreted in the form of urea, while the carbon backbone is used for gluconeogenesis. The key
390 enzyme for the Cahill-cycle is ALT, conventionally associated with muscle and liver (29, 30). Previously,
391 ALT was found in glial cells of the honeybee retina (44), and ALT activity was detected in rat retinal tissue
392 lysates (45). In our study, the localization of ALT in photoreceptors and inner retinal neurons, combined
393 with our interventional and metabolomic datasets, demonstrated the operation of the Cahill-cycle in the
394 mammalian retina. Moreover, the expression of mitochondrial PCK2 in cones facilitates the efficient
395 uncoupling of glycolysis from the Krebs-cycle, suggesting that cones may use the Cahill-cycle for very
396 effective energy production.

397

398 **Glutamine from MGCs provides additional fuel for cones**

399 MGCs are known for their uptake of extracellular glutamate and use for glutamine synthesis. In fact, in
400 retinal histology, glutamate-aspartate transporter (GLAST) and glutamine synthase (GS) have been widely
401 used as markers for MGCs (25, 34). Glutaminase C (GAC) converts glutamine back to glutamate, which
402 may then serve as a substrate for the mini-Krebs-cycle. We localized GAC in inner retinal neurons and
403 photoreceptors, with a particularly strong expression in cone inner segments. Here, GAC overlaps with
404 ALT expression, indicating that cones can use glutaminolysis to obtain extra glutamate for pyruvate
405 transamination in the Cahill-cycle. This may also explain why the glycolysis inhibitor Shikonin reduced
406 cone viability much less than that of rods.

407

408 **A hypotaurine-taurine shuttle can transfer NADH from RPE to photoreceptors**

409 The regeneration of the photoreceptor photopigment retinal is performed by the RPE (12). Recently,
410 retinal has been proposed to form a Schiff base adduct with taurine, which would act as a retinal carrier
411 and buffer (46). We found that retina cultured with RPE harbored high levels of taurine and low levels of
412 hypotaurine, while retina without RPE displayed low levels of taurine and high levels of hypotaurine. Our
413 taurine immunostaining found essentially no taurine in the RPE, while photoreceptor inner segments and
414 synapses displayed very high taurine levels. Together, these findings suggest a hypotaurine-taurine
415 shuttle between RPE and photoreceptors. In the RPE taurine can be reduced to hypotaurine and shuttled
416 back to photoreceptors where oxidation by hypotaurine dehydrogenase (46, 47) may reconstitute taurine,
417 yielding additional NADH for OXPHOS. The net effect of this hypotaurine-taurine shuttle would be a
418 transfer of reducing power from RPE to photoreceptors, boosting photoreceptor ATP production via
419 OXPHOS.

420

421 **Rods use the mini-Krebs-cycle to uncouple glycolysis from mitochondrial metabolism**

422 A key problem in the understanding of cellular energy metabolism is the relationship between fast but
423 inefficient glycolysis and slow but efficient Krebs-cycle/OXPHOS (48, 49). Both pathways are coupled via
424 pyruvate and the different metabolic flow rates reduce the efficiency of energy production, *e.g.*, via
425 feedback inhibition (50). Pyruvate coupling is especially problematic in high and rapidly changing energy
426 demand such as in neurons and photoreceptors (51). Uncoupling glycolysis and Krebs-cycle via the Cori-
427 cycle is extremely wasteful and likely insufficient to satisfy long-term photoreceptor energy demand. By

428 comparison, the Cahill-cycle delivers additional NADH when using pyruvate derived from glycolysis, and
429 cones may use the Cahill-cycle for uncoupling from glycolysis. An alternative pathway is the mini-Krebs-
430 cycle, essentially an oxalacetate to α-ketoglutarate shunt (28). This cycle uses glutamate, glutamine, and
431 BCAAs as fuels to run mitochondrial respiration independent of glycolysis. The key step of the mini-Krebs-
432 cycle is the transamination of oxaloacetate/glutamate to aspartate/α-ketoglutarate by AAT. α-
433 Ketoglutarate is then metabolized to oxaloacetate, generating NADH, $FADH_2$, and GTP. Acetyl-CoA
434 generated from BCAAs or pyruvate is used to create NAA, the end product of the mini-Krebs-cycle. We
435 found mitochondrial AAT2 to be expressed in rod inner segments, in agreement with an early
436 cytochemical study (52). This indicates that the mini-Krebs-cycle is used primarily by rods, explaining their
437 selective vulnerability to FCCP treatment. Crucially, the mini-Krebs-cycle is more energy-efficient than the
438 Cahill-cycle and generates NAA instead of alanine as net product. Both metabolites serve the purpose of
439 disposing of excess ammonia originating from AA input (53, 54). NAA in the human brain is one of the
440 most abundant metabolites and is routinely used in clinical MRI diagnosis to visualize brain health (55).
441 While different functions have been hypothesized for NAA (56, 57), our work proposes NAA as a signature
442 metabolite for the mini-Krebs-cycle. Indeed, a recent study using Raman spectroscopy imaging detected
443 high levels of NAA in the human retina, demonstrating *in vivo* use of this cycle (58). Importantly, the 6-
444 step mini-Krebs-cycle is significantly faster than the 10-step Krebs-cycle (28), more energy-efficient, and
445 uncoupled from glycolysis. In rods, PCK1 may allow to replenish cytoplasmic acetyl-CoA pools from
446 oxaloacetate, if BCAA-derived input was insufficient.

447 Overall, the different pathways outlined here provide photoreceptor cells with remarkable versatility and
448 flexibility, notably in terms of substrate use, allowing them to dynamically adapt the timing and
449 quantitative output of energy metabolism. Rods rely strongly on the Krebs-cycle and OXPHOS, while cones
450 are more dependent on glycolysis. These differences between rod and cone metabolism may be related
451 to their response kinetics and sensitivities. The flexible uncoupling of glycolysis from mitochondrial
452 respiration, allows both processes to run at optimum, producing the characteristic signature metabolites
453 lactate (Cori-cycle), alanine (Cahill-cycle), and NAA (mini-Krebs-cycle). These metabolites can reveal
454 energy or disease status and could serve as readout and guide for the design of novel therapeutic
455 interventions. Given the general importance of energy metabolism, the significance of our findings
456 extends beyond the retina, for instance, to other neurodegenerative and metabolic diseases.

457

## Materials and Methods

C3H wild-type (WT) mice were used to generate organotypic retinal explant cultures (18). All efforts were made to minimize the number of animals used and their suffering. Protocols compliant with the German law on animal protection were reviewed and approved by the ''Einrichtung fur Tierschutz, Tierärztlichen Dienst und Labortierkunde'' of the University of Tübingen and were following the association for research in vision and ophthalmology (ARVO) statement for the use of animals in vision research. For details on the experimental procedures, immunofluorescence, and antibodies, as well as metabolomic analysis and databases used please refer to the supporting information (SI).

## Declarations

### Ethics approval and consent to participate

Protocols compliant with the German law on animal protection were reviewed and approved by the institution for animal welfare, veterinary service and laboratory animal science (Einrichtung für Tierschutz, Tierärztlichen Dienst und Labortierkunde) of the University of Tübingen and were following the association for research in vision and ophthalmology (ARVO) statement for the use of animals in vision research.

### Availability of data and materials

Raw NMR spectroscopy data is available upon request. Any additional information required to reanalyze the data reported in this paper is available from the lead contact upon request. This paper does not report original code.

### Competing interests

The authors declare no competing financial interests. CT reports a research grant by Bruker BioSpin GmbH.,

### Funding

This work was funded by the ProRetina Foundation, the Zinke heritage foundation, the Werner Siemens Foundation, the Chinese scholarship council (CSC), ANID-FONDECYT No. 1210790 (OS) and PhD grant BECAS CHILE/2018 -21180443 (VC).

### CRediT author contribution statement

**Yiyi Chen**: Conceptualization, Methodology, Investigation, Writing – original draft. **Laimdota Zizmare**: Conceptualization, Methodology, Investigation, Writing – original draft. **François Paquet-Durand**: Conceptualization, Methodology, Investigation, Writing – original draft, Writing – Review & Editing, Supervision, Funding acquisition. **Christoph Trautwein**: Conceptualization, Methodology, Investigation, Writing – original draft, Writing – Review & Editing, Supervision, Funding acquisition. **Shirley Yu**: Investigation. **Lan Wang**: Investigation. **Friedrich W. Herberg**: Writing – Review & Editing. **Oliver Schmachtenberg**: Writing – Review & Editing. **Victor Calbiague**: Writing – Review & Editing.

## Acknowledgements

We thank N. Rieger and M. Owczorz for first-rate technical support as well as James B. Hurley and Daniel Hass (both University of Washington, Seattle, USA) for helpful comments and suggestions.

## References

1. M. W. Country, Retinal metabolism: A comparative look at energetics in the retina. Brain Res 1672, 50-57 (2017).

2. M. T. Wong-Riley, Energy metabolism of the visual system. Eye Brain 2, 99-116 (2010).

3. A. Swarup et al., Modulating GLUT1 expression in retinal pigment epithelium decreases glucose levels in the retina: impact on photoreceptors and Müller glial cells. Am J Physiol Cell Physiol 316, C121-c133 (2019).

4. O. Warburg, The metabolism of carcinoma cells. The Journal of Cancer Research 9, 148-163 (1925).

5. H. Okawa, A. P. Sampath, S. B. Laughlin, G. L. Fain, ATP consumption by mammalian rod photoreceptors in darkness and in light. Curr Biol 18, 1917-1921 (2008).

6. A. Ames, 3rd, Energy requirements of CNS cells as related to their function and to their vulnerability to ischemia: a commentary based on studies on retina. Can J Physiol Pharmacol 70 Suppl, S158-164 (1992).

7. Y. Chinchore, T. Begaj, D. Wu, E. Drokhlyansky, C. L. Cepko, Glycolytic reliance promotes anabolism in photoreceptors. Elife 6 (2017).

8. R. W. Young, The renewal of photoreceptor cell outer segments. J Cell Biol 33, 61-72 (1967).

9. N. T. Ingram, G. L. Fain, A. P. Sampath, Elevated energy requirement of cone photoreceptors. Proceedings of the National Academy of Sciences 117, 19599-19603 (2020).

10. D. Sacks et al., Multisociety Consensus Quality Improvement Revised Consensus Statement for Endovascular Therapy of Acute Ischemic Stroke. Int J Stroke 13, 612-632 (2018).

11. M. A. Kanow et al., Biochemical adaptations of the retina and retinal pigment epithelium support a metabolic ecosystem in the vertebrate eye. Elife 6 (2017).

12. T. M. Redmond et al., Rpe65 is necessary for production of 11-cis-vitamin A in the retinal visual cycle. Nat Genet 20, 344-351 (1998).

13. K. Takata, T. Kasahara, M. Kasahara, O. Ezaki, H. Hirano, Ultracytochemical localization of the erythrocyte/HepG2-type glucose transporter (GLUT1) in cells of the blood-retinal barrier in the rat. Invest Ophthalmol Vis Sci 33, 377-383 (1992).

14. I. A. Simpson et al., The facilitative glucose transporter GLUT3: 20 years of distinction. Am J Physiol Endocrinol Metab 295, E242-253 (2008).

15. J. M. Rhoads et al., L-glutamine stimulates intestinal cell proliferation and activates mitogen-activated protein kinases. Am J Physiol 272, G943-953 (1997).

16. R. J. Kessler, C. A. Tyson, D. E. Green, Mechanism of uncoupling in mitochondria: uncouplers as ionophores for cycling cations and protons. Proc Natl Acad Sci U S A 73, 3141-3145 (1976).

17. S. Belhadj et al., Long-Term, Serum-Free Cultivation of Organotypic Mouse Retina Explants with Intact Retinal Pigment Epithelium. J Vis Exp 10.3791/61868 (2020).

18. H. G. Joost, A. D. Habberfield, I. A. Simpson, A. Laurenza, K. B. Seamon, Activation of adenylate cyclase and inhibition of glucose transport in rat adipocytes by forskolin analogues: structural determinants for distinct sites of action. Mol Pharmacol 33, 449-453 (1988).

542 19. X. Zhao et al., Shikonin Inhibits Tumor Growth in Mice by Suppressing Pyruvate Kinase M2-
543 mediated Aerobic Glycolysis. Scientific Reports 8, 14517 (2018).

544 20. A. Ortin-Martinez et al., Number and distribution of mouse retinal cone photoreceptors:
545 differences between an albino (Swiss) and a pigmented (C57/BL6) strain. PloS one 9, e102392 (2014).

546 21. C. J. Jeon, E. Strettoi, R. H. Masland, The major cell populations of the mouse retina. J Neurosci
547 18, 8936-8946 (1998).

548 22. P. Felig, The glucose-alanine cycle. Metabolism 22, 179-207 (1973).

549 23. P. Bai, Biology of Poly(ADP-Ribose) Polymerases: The Factotums of Cell Maintenance. Mol Cell 58,
550 947-958 (2015).

551 24. F. Paquet-Durand et al., Excessive activation of poly(ADP-ribose) polymerase contributes to
552 inherited photoreceptor degeneration in the retinal degeneration 1 mouse. J Neurosci 27, 10311-10319
553 (2007).

554 25. R. E. Riepe, M. D. Norenburg, Müller cell localisation of glutamine synthetase in rat retina. Nature
555 268, 654-655 (1977).

556 26. M. M. Giarmarco et al., Daily mitochondrial dynamics in cone photoreceptors. Proc Natl Acad Sci
557 U S A 117, 28816-28827 (2020).

558 27. B. A. Zabel et al., Human G protein–coupled receptor GPR-9-6/CC chemokine receptor 9 is
559 selectively expressed on intestinal homing T lymphocytes, mucosal lymphocytes, and thymocytes and is
560 required for thymus-expressed chemokine–mediated chemotaxis. The Journal of experimental medicine
561 190, 1241-1256 (1999).

562 28. M. Yudkoff, D. Nelson, Y. Daikhin, M. Erecińska, Tricarboxylic acid cycle in rat brain
563 synaptosomes. Fluxes and interactions with aspartate aminotransferase and malate/aspartate shuttle. J
564 Biol Chem 269, 27414-27420 (1994).

565 29. R. A. Nathwani, S. Pais, T. B. Reynolds, N. Kaplowitz, Serum alanine aminotransferase in skeletal
566 muscle diseases. Hepatology 41, 380-382 (2005).

567 30. W. R. Kim, S. L. Flamm, A. M. Di Bisceglie, H. C. Bodenheimer, Serum activity of alanine
568 aminotransferase (ALT) as an indicator of health and disease. Hepatology 47, 1363-1370 (2008).

569 31. T. Sinha, M. I. Naash, M. R. Al-Ubaidi, The Symbiotic Relationship between the Neural Retina and
570 Retinal Pigment Epithelium Is Supported by Utilizing Differential Metabolic Pathways. iScience 23, 101004
571 (2020).

572 32. C. F. Cori, G. T. Cori, Carbohydrate metabolism. Annu Rev Biochem 15, 193-218 (1946).

573 33. R. V. S. Rajala, Aerobic Glycolysis in the Retina: Functional Roles of Pyruvate Kinase Isoforms.
574 Frontiers in Cell and Developmental Biology 8 (2020).

575 34. E. M. Rueda et al., The cellular and compartmental profile of mouse retinal glycolysis,
576 tricarboxylic acid cycle, oxidative phosphorylation, and ~P transferring kinases. Molecular vision 22, 847-
577 885 (2016).

578 35. F. O'Leary, M. Campbell, The blood-retina barrier in health and disease. Febs j
579 10.1111/febs.16330 (2021).

580 36. R. Diaz-Ruiz, M. Rigoulet, A. Devin, The Warburg and Crabtree effects: On the origin of cancer cell
581 energy metabolism and of yeast glucose repression. Biochimica et Biophysica Acta (BBA) - Bioenergetics
582 1807, 568-576 (2011).

583 37. H. G. Crabtree, Observations on the carbohydrate metabolism of tumours. Biochem J 23, 536-545
584 (1929).

585 38. G. U. Balcke et al., Linking energy metabolism to dysfunctions in mitochondrial respiration--a
586 metabolomics in vitro approach. Toxicol Lett 203, 200-209 (2011).

587 39. L. L. Dugan et al., Mitochondrial production of reactive oxygen species in cortical neurons
588 following exposure to N-methyl-D-aspartate. J Neurosci 15, 6377-6388 (1995).

589 40. V. Schreiber, F. Dantzer, J. C. Ame, G. de Murcia, Poly(ADP-ribose): novel functions for an old
590 molecule. Nat Rev Mol Cell Biol 7, 517-528 (2006).

591 41. A. Venkatesh et al., Activated mTORC1 promotes long-term cone survival in retinitis pigmentosa
592 mice. J Clin Invest 125, 1446-1458 (2015).

593 42. N. Aït-Ali et al., Rod-derived cone viability factor promotes cone survival by stimulating aerobic
594 glycolysis. Cell 161, 817-832 (2015).

595 43. M. Yang et al., Expression of glucose transporter-2 in murine retina: Evidence for glucose
596 transport from horizontal cells to photoreceptor synapses. J Neurochem 160, 283-296 (2022).

597 44. M. Tsacopoulos, A. L. Veuthey, S. G. Saravelos, P. Perrottet, G. Tsoupras, Glial cells transform
598 glucose to alanine, which fuels the neurons in the honeybee retina. J Neurosci 14, 1339-1351 (1994).

599 45. K. F. LaNoue et al., Role of specific aminotransferases in de novo glutamate synthesis and redox
600 shuttling in the retina. J Neurosci Res 66, 914-922 (2001).

601 46. S. Veeravalli et al., Flavin-Containing Monooxygenase 1 Catalyzes the Production of Taurine from
602 Hypotaurine. Drug Metab Dispos 48, 378-385 (2020).

603 47. K. Sumizu, Oxidation of hypotaurine in rat liver. Biochim Biophys Acta 63, 210-212 (1962).

604 48. J. Zheng, Energy metabolism of cancer: Glycolysis versus oxidative phosphorylation (Review).
605 Oncol Lett 4, 1151-1157 (2012).

606 49. T. Pfeiffer, S. Schuster, S. Bonhoeffer, Cooperation and competition in the evolution of ATP-
607 producing pathways. Science 292, 504-507 (2001).

608 50. J. C. Lai, K. L. Behar, Glycolysis-citric acid cycle interrelation: a new approach and some insights in
609 cellular and subcellular compartmentation. Dev Neurosci 15, 181-193 (1993).

610 51. J. Du et al., Phototransduction Influences Metabolic Flux and Nucleotide Metabolism in Mouse
611 Retina. J Biol Chem 291, 4698-4710 (2016).

612 52. R. Gebhard, Cytochemical demonstration of aspartate aminotransferase activity in the rat retina.
613 Brain Res 539, 337-341 (1991).

614 53. J. R. Moffett, B. Ross, P. Arun, C. N. Madhavarao, A. M. A. Namboodiri, N-Acetylaspartate in the
615 CNS: from neurodiagnostics to neurobiology. Progress in neurobiology 81, 89-131 (2007).

616 54. S. Dadsetan et al., Brain alanine formation as an ammonia-scavenging pathway during
617 hyperammonemia: effects of glutamine synthetase inhibition in rats and astrocyte-neuron co-cultures. J
618 Cereb Blood Flow Metab 33, 1235-1241 (2013).

619 55. H. Igarashi, Y. Suzuki, V. J. Huber, M. Ida, T. Nakada, N-acetylaspartate decrease in acute stage of
620 ischemic stroke: a perspective from experimental and clinical studies. Magn Reson Med Sci 14, 13-24
621 (2015).

622 56. H. D. Yan, K. Ishihara, T. Serikawa, M. Sasa, Activation by N-acetyl-L-aspartate of acutely
623 dissociated hippocampal neurons in rats via metabotropic glutamate receptors. Epilepsia 44, 1153-1159
624 (2003).

625 57. J. Moffett, P. Arun, P. Ariyannur, A. Namboodiri, N-Acetylaspartate reductions in brain injury:
626 impact on post-injury neuroenergetics, lipid synthesis, and protein acetylation. Frontiers in
627 Neuroenergetics 5 (2013).

628 58. S. Alba-Arbalat et al., In Vivo Molecular Changes in the Retina of Patients With Multiple Sclerosis.
629 Investigative ophthalmology & visual science 62, 11-11 (2021).

## Figures and Tables

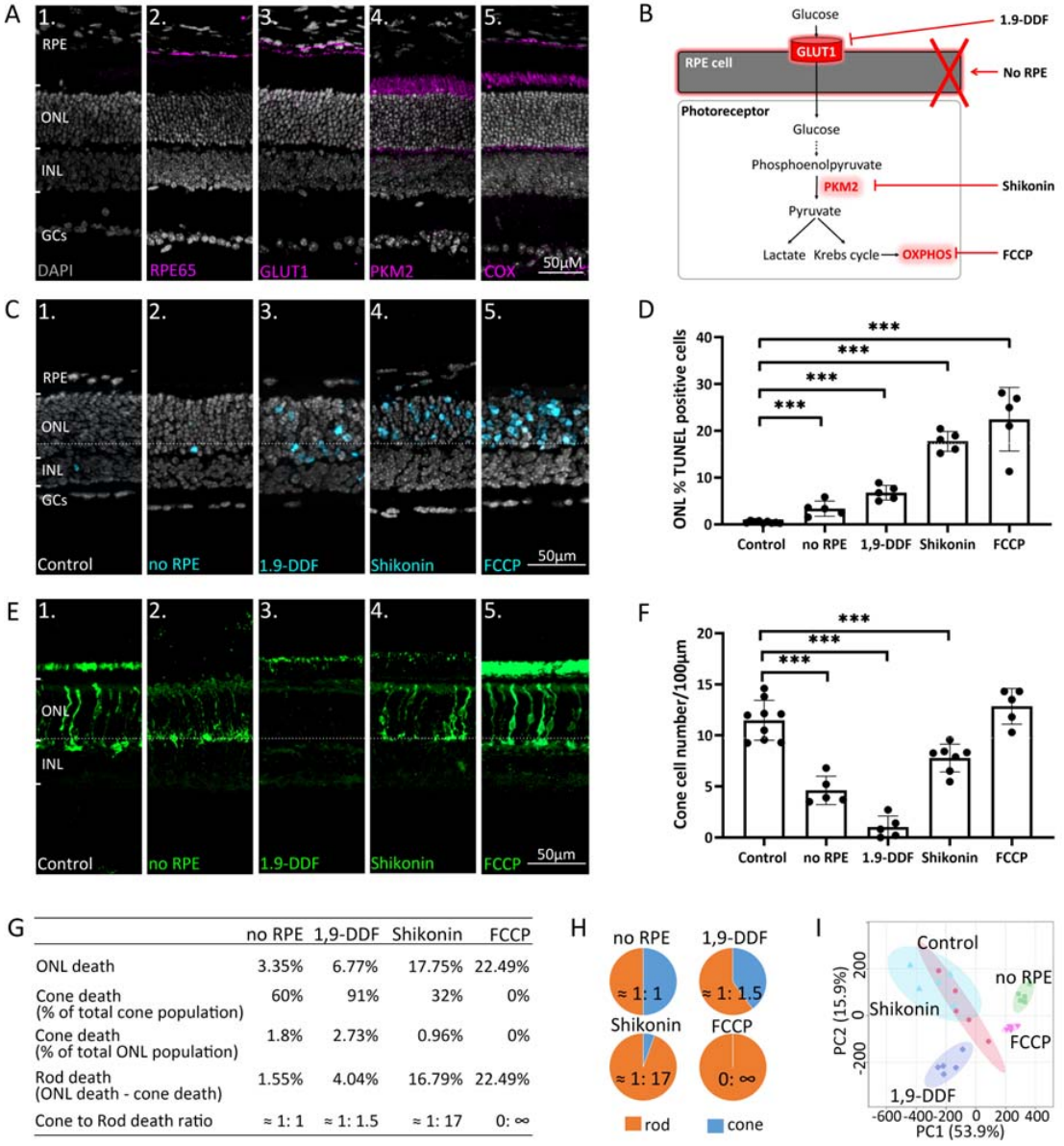


| | no RPE | 1,9-DDF | Shikonin | FCCP |
|---|---|---|---|---|
| ONL death | 3.35% | 6.77% | 17.75% | 22.49% |
| Cone death (% of total cone population) | 60% | 91% | 32% | 0% |
| Cone death (% of total ONL population) | 1.8% | 2.73% | 0.96% | 0% |
| Rod death (ONL death - cone death) | 1.55% | 4.04% | 16.79% | 22.49% |
| Cone to Rod death ratio | ≈ 1: 1 | ≈ 1: 1.5 | ≈ 1: 17 | 0: ∞ |

**Figure 1. Manipulating energy metabolism differentially affects rod and cone photoreceptors.** (A) Immunofluorescence staining (magenta): (A1) negative control, (A2) RPE65, (A3) glucose transporter-1 (GLUT1), (A4) pyruvate kinase M2 (PKM2), (A5) mitochondrial cytochrome oxidase (COX). (B) Overview of experimental manipulations. Organotypic retinal explants were cultured with or without RPE or treated with 1,9-DDF, Shikonin, or FCCP. (C) TUNEL assay (cyan) marking dying cells in the five experimental conditions. (D) Quantification of TUNEL-positive cells in outer nuclear layer (ONL). Data represented as mean ± SD. (E) Cone-arrestin labelling (green) in the ONL. (F) Quantification of arrestin-positive cones. Data represented as mean ± SD. (G) Table giving percentages of cones and rods lost for each treatment. (H) Pie charts illustrate cone to rod cell death ratios. (I) Principal component analysis (PCA) of retinal samples investigated with $^{1}$H-NMR spectroscopy-based metabolomics. Dots in graphs represent individual retinal explants. Asterisks indicate significance levels: *p<0.05, **p<0.01, *** p<0.001. RPE = retinal pigment epithelium; INL = inner nuclear layer; GCs = ganglion cells.

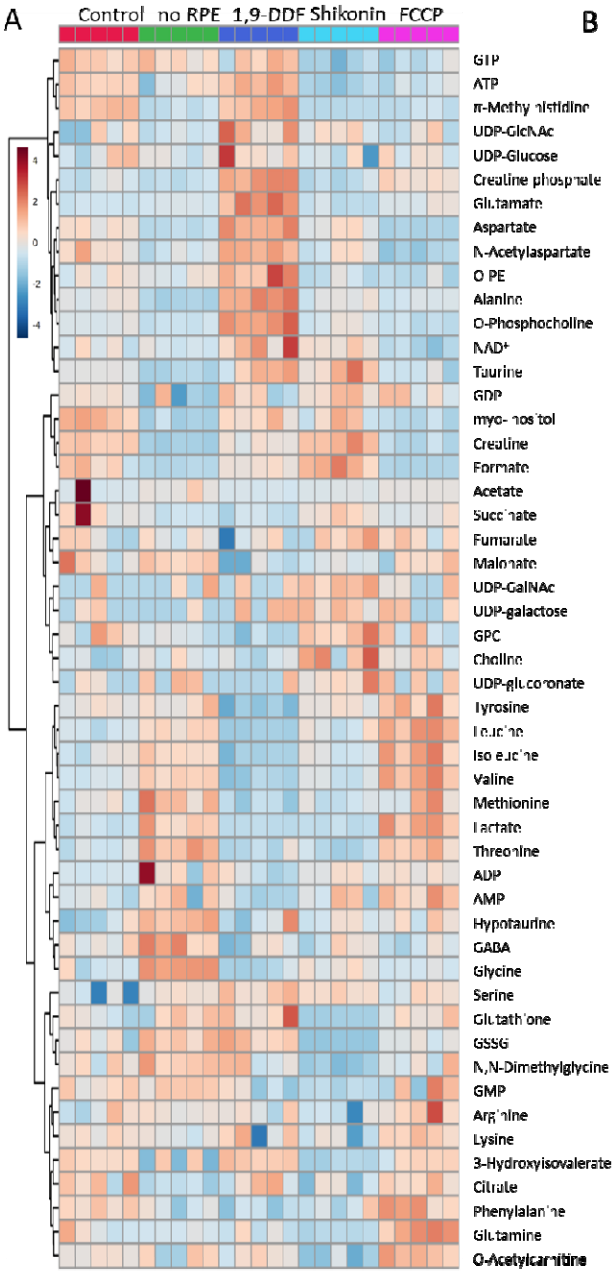


| Class | Function | Metabolite | no RPE | | 1,9-DDF | | Shikonin | | FCCP | |
|---|---|---|---|---|---|---|---|---|---|---|
| | | | p | FC | p | FC | p | FC | p | FC |
| Nucleotides | Energy metabolism, cofactors | **ATP** | ↓* | 0.8 | ↑** | 1.1 | ↓**** | 0.6 | ↓*** | 0.7 |
| | | **ADP** | | | | | ↑* | 1.3 | ↑*** | 1.5 |
| | | **AMP** | | | | | | | ↑** | 1.8 |
| | | **GTP** | | | | | ↓**** | 0.6 | ↓*** | 0.7 |
| | | **GDP** | | | | | | | | |
| | | **GMP** | | | | | ↓*** | 0.4 | | |
| | Coenzyme | **NAD+** | | | ↑* | 1.3 | | | ↓* | 0.8 |
| | | **UDP-GalNAc** | | | | | ↑* | 3.2 | | |
| | | **UDP-GlcNAc** | | | ↑* | 1.5 | | | | |
| Organic Acids | Glycolysis | Lactate | ↑*** | 9.7 | | | | | ↑**** | 4.6 |
| | Krebs cycle | Citrate | ↓* | 0.7 | | | | | | |
| | | Fumarate | | | | | | | | |
| | | Succinate | | | | | | | | |
| | Mitochondria | Formate | ↓** | 0.7 | | | | | ↓** | 0.7 |
| | Osmolyte | Taurine | ↓**** | 0.9 | ↑* | 1.1 | ↑* | 1.1 | | |
| | | Hypotaurine | ↑*** | 1.9 | | | | | | |
| | Neurona tissue-associated metabolite | GABA | ↑** | 1.1 | | | | | | |
| | | Malonate | | | ↓* | 0.4 | | | | |
| | | NAA | ↓* | 0.8 | ↑* | 1.2 | | | ↓*** | 0.6 |
| | | Creatine | ↓**** | 0.6 | ↓*** | 0.9 | | | ↓*** | 0.6 |
| | | Creatine phosphate | | | ↑**** | 1.6 | | | ↑** | |
| Amino Acids | Neuro-transmitter, Krebs cycle | Glutamate | ↑** | 1.1 | ↑**** | 2.1 | | | ↑** | 1.2 |
| | BCAA | Isoleucine | ↑** | 1.3 | ↓** | 0.7 | | | ↑** | 1.6 |
| | | Leucine | ↑*** | 1.3 | ↓** | 0.8 | | | ↑*** | 1.5 |
| | | Valine | ↑**** | 1.3 | ↓** | 0.8 | | | ↑*** | 1.5 |
| | Glucogenic, ketogenic amino acid | Glutamine | | | | | ↓* | 0.7 | ↑* | 1.5 |
| | | Tyrosine | | | ↓**** | 0.7 | | | ↑* | 1.2 |
| | | Lysine | | | | | | | ↑* | 1.1 |
| | | Phenylalanine | ↓* | 0.9 | ↓** | 0.8 | ↓* | 0.9 | | |
| | | **Aspartate** | ↓**** | 0.6 | ↑** | 1.6 | | | ↓*** | 0.4 |
| | | **Alanine** | ↓**** | 0.8 | ↑**** | 1.5 | | | ↓** | 0.9 |
| | Serine synthesis pathway, one carbon metabolism | Methionine | ↑** | 2.1 | ↓* | 0.4 | | | | |
| | | Serine | ↑* | 1.7 | ↑* | 2.0 | ↑* | 1.8 | | |
| | | Glycine | ↑**** | 1.6 | | | | | | |
| | | Threonine | ↑**** | 1.4 | | | | | ↑*** | 1.3 |
| | | π-Methyl-histidine | ↓**** | 0.2 | | | ↓**** | 0.1 | ↓*** | 0.2 |
| | | N,N-Dimethyl-glycine | ↑* | 1.2 | | | ↓** | 0.6 | | |
| Lipids and growth | β-oxidation of fatty acids | O-Acetyl-carnitine | | | | | ↓** | 0.5 | ↑** | 1.4 |
| | | 3-Hydroxy-isovalerate | | | ↑* | 1.1 | ↓**** | 0.5 | | |
| | Cell membrane synthesis, Kennedy pathway | myo-Inositol | ↓**** | 0.6 | | | | | ↓*** | 0.6 |
| | | Choline | | | | | ↑* | 1.7 | ↑* | 1.3 |
| | | O-Pospho-choline | ↓** | 0.8 | ↑**** | 2.0 | | | ↓** | 0.8 |
| | | GPC | | | ↓* | 0.8 | | | | |
| | | O-PE | | | ↑** | 1.3 | ↓* | 0.9 | ↓* | 0.9 |
| Tri-peptide | Redox metabolism | Glutathione | | | | | ↓** | 0.1 | | |
| | | GSSG | ↑* | 1.8 | ↑* | 1.8 | ↓** | 0.1 | | |

**Figure 2. $^{1}$H-NMR spectroscopy-based metabolomic analysis of retina subjected to interventions in energy metabolism.** (A) Heatmap based on unsupervised hierarchical cluster analysis by Ward's linkage, showing auto-scaled metabolite concentrations (red – high, blue – low) in five different experimental conditions: control - red, *no* RPE - green, 1,9-DDF - dark blue, Shikonin - light blue, FCCP purple (n = 5 samples per condition). (B) Metabolic profiles of each intervention were compared to control. Metabolites significantly changed in at least one experimental condition were grouped according to functions and pathways. Data show p-values and fold change (FC) over control. Statistical comparison: student´s unpaired t-test (group variance equal); p-values: **** < 0.0001, *** < 0.001, ** < 0.01 * < 0.05. See also Supplementary Figure 2.

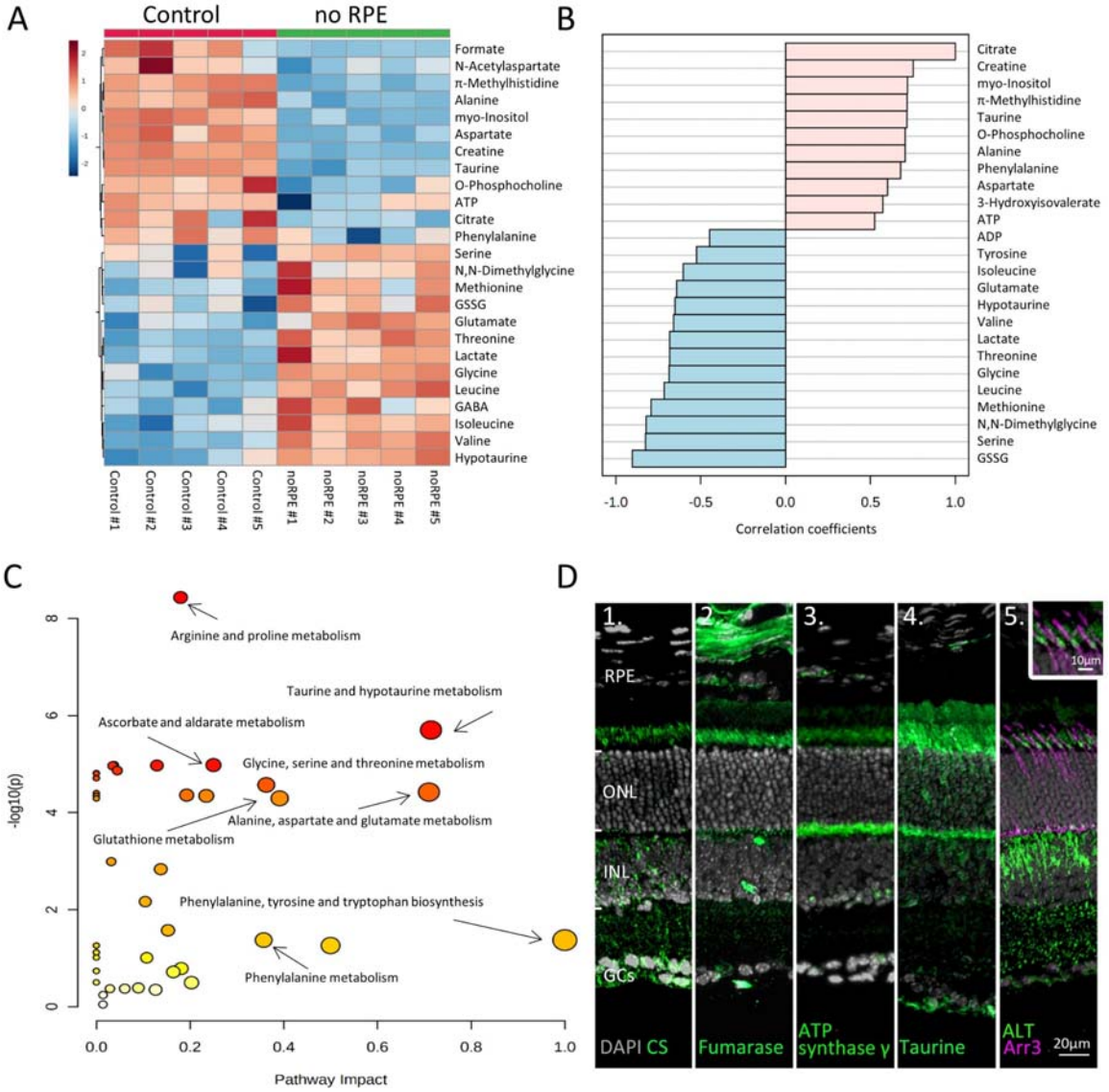


**Figure 3. Absence of RPE dramatically changes retinal metabolism.** (A) Heatmap, based on unsupervised hierarchical cluster analysis by Ward's linkage, illustrating statistically significant changes for 25 metabolites (unpaired t-test, fold change (FC) > 1.2, raw p value < 0.05). (B) Pattern hunter for citrate, showing the top 25 correlating metabolites, correlation coefficient given as Pearson r distance. (C) Metabolic pathways most affected in *no* RPE condition compared to control, based on KEGG- pathway database. (D) Immunodetection of enzymes and metabolites (green): (D1) citrate synthase (CS), (D2) fumarase, (D3), ATP synthase γ, (D4) taurine, (D5) alanine transaminase (ALT). Co-staining for ALT and cone arrestin (Arr3; magenta) showed high expression in cone inner segments. DAPI (grey) was used as a nuclear counterstain. See also Supplementary Figure 3.

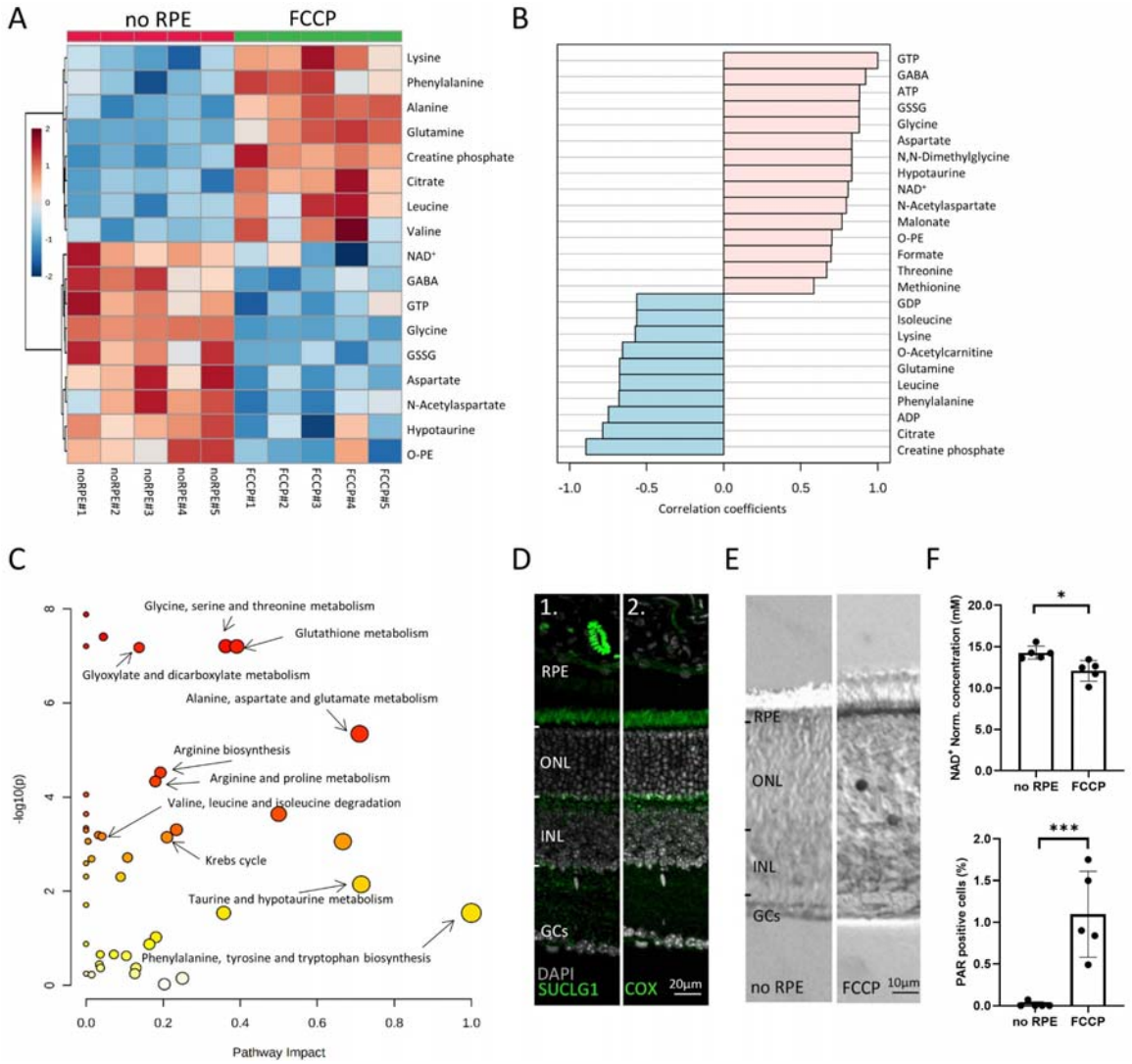


**Figure 4. Comparison between *no* RPE and FCCP conditions.** (A) Heatmap, based on unsupervised hierarchical cluster analysis by Ward's linkage, illustrating statistically significant metabolite changes (unpaired t-test, fold change > 1.2, raw p-value < 0.05). (B) Pattern hunter for guanosine triphosphate (GTP) showing the top 25 correlating compounds. Correlation coefficient given as Pearson r distance. (C) KEGG-based pathway analysis, comparison between *no* RPE and FCCP. (D) Immunofluorescence for succinate-CoA ligase-1 (SUCLG1, green) labelled photoreceptor inner segments and colocalized with COX. DAPI (grey) was used as a nuclear counterstain. (E) PAR positive photoreceptors (black) in the outer nuclear layer (ONL) of FCCP treated retina. (F) Compared to *no* RPE, $NAD^+$ levels were lower in the FCCP group, while the percentage of PAR positive cells was higher. Data represented as mean ± SD. p values: *** < 0.001, * < 0.05. See also Supplementary Figure 5.

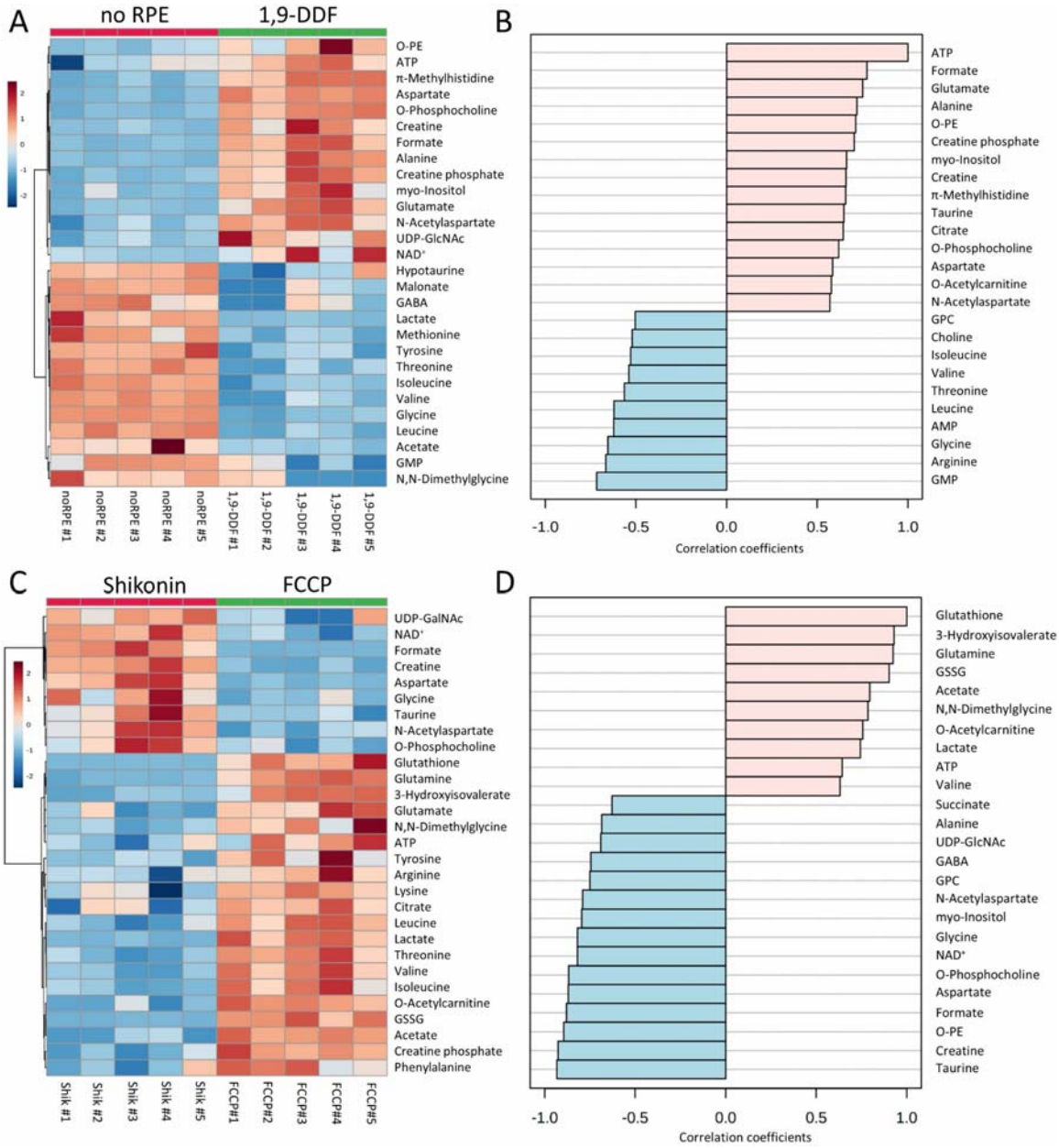


**Figure 5. Metabolomic analysis of *no* RPE vs. 1,9-DDF treatment and Shikonin vs. FCCP treatment.** Heatmap illustrating statistically significant metabolite changes (unpaired t-test, fold change (FC) > 1.2, raw p value < 0.05) for (A) *no* RPE vs. 1,9-DDF and (C) Shikonin vs. FCCP. Pattern hunter for (B) ATP and (D) glutathione, showing the top 25 correlating compounds. Correlation coefficient given as Pearson r distance. See also Supplementary Figures 6 and 7.

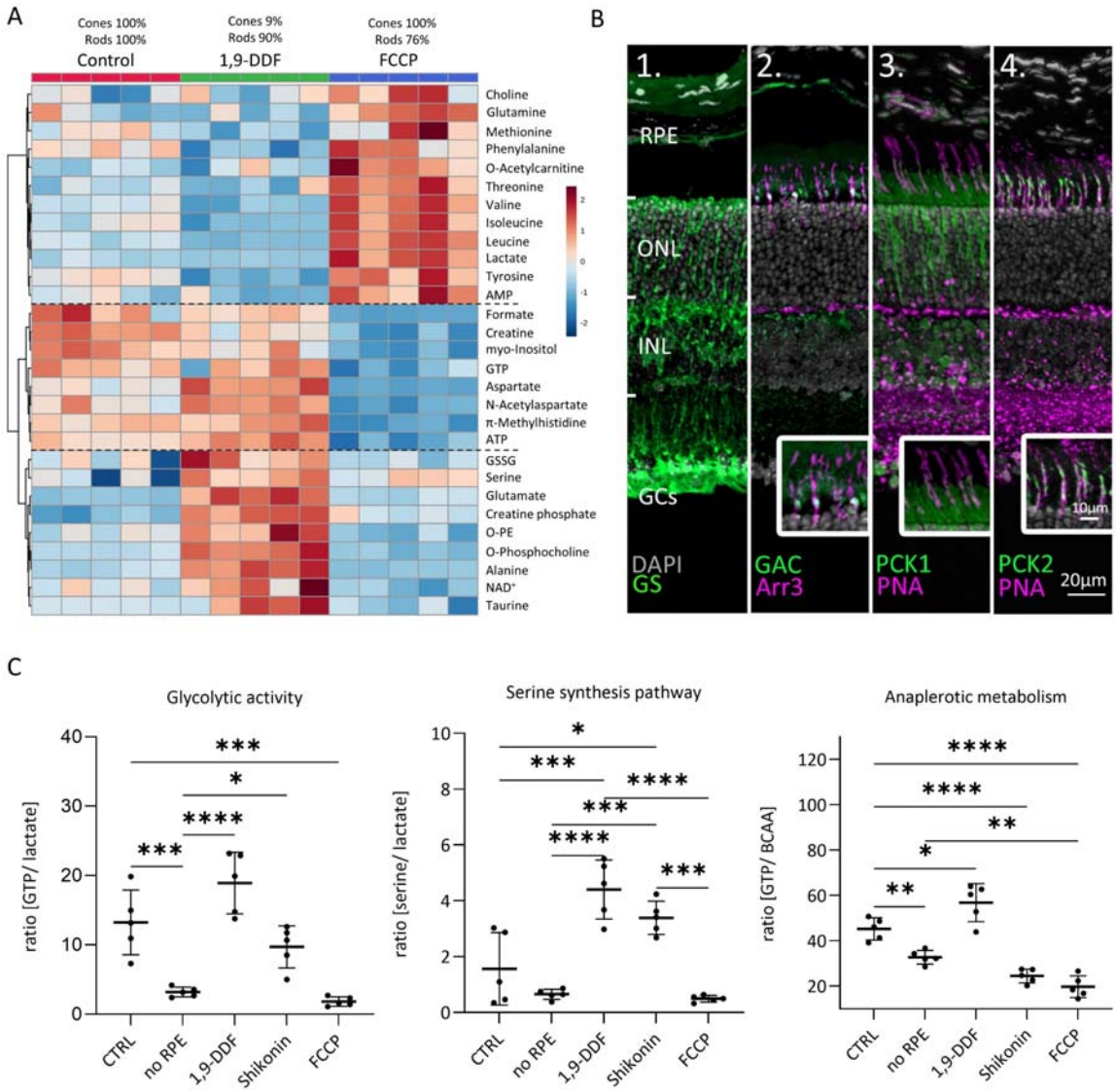


**Figure 6. Metabolomic comparison between control, 1,9-DDF, and FCCP treatment.** (A) Heatmap illustrating 29 statistically significant metabolite changes (parametric one-way ANOVA, Fisher's LSD post-hoc analysis). Three main clusters of metabolite changes were evident (dashed lines). (B) Immunostaining (green) for enzymes related to glutamine metabolism. DAPI (grey) was used as nuclear counterstain. (B1) Glutamine synthase (GS), (B2) glutaminase C (GAC); co-localization with cone-arrestin (Arr3; magenta). (B3) phosphoenolpyruvate carboxykinase 1 (PCK1) and (B4) PCK2, both co-localized with cone marker peanut-agglutinin (PNA). (C) Ratios between metabolites representing glycolysis (lactate vs. GTP), anaplerotic metabolism (GTP vs. BCAA), and serine synthesis pathway (serine vs. lactate). Data represented as individual data points with mean ± SD. Statistical comparison using one-way ANOVA, Tukey's multiple comparisons test; p values: **** < 0.0001, *** < 0.001, ** < 0.01 * < 0.05. See also Supplementary Figure 8.

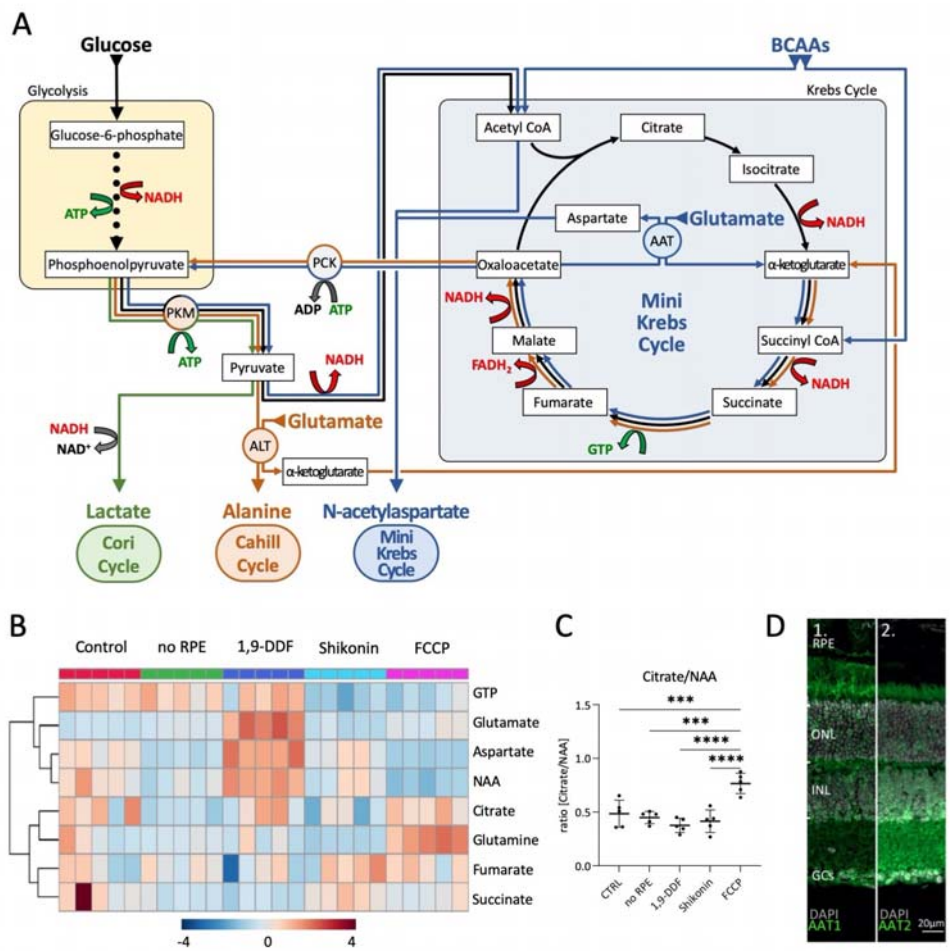


**Figure 7. Metabolic pathways in the retina, key metabolites, and expression of aspartate amino transferase (AAT).** (A) Overview of main metabolic pathways and metabolites. Execution of Cori- (green arrows), Cahill- (brown), or mini-Krebs-cycle (blue) releases the signature metabolites lactate, alanine, and N-acetylaspartate (NAA), respectively. Key enzymes of the Cahill- and mini-Krebs-cycle are phosphoenolpyruvate carboxykinase (PCK), pyruvate kinase M (PKM), alanine transaminase (ALT) and AAT. (B) Hierarchical clustering of eight metabolites connected to Krebs and mini-Krebs cycle. (C) Ratio NAA *vs*. citrate, representing full and mini-Krebs-cycle. Data represented as ratio of individual data points with mean ± SD. (D) AAT-1 and -2 staining (green) with DAPI (grey) as nuclear counterstain.

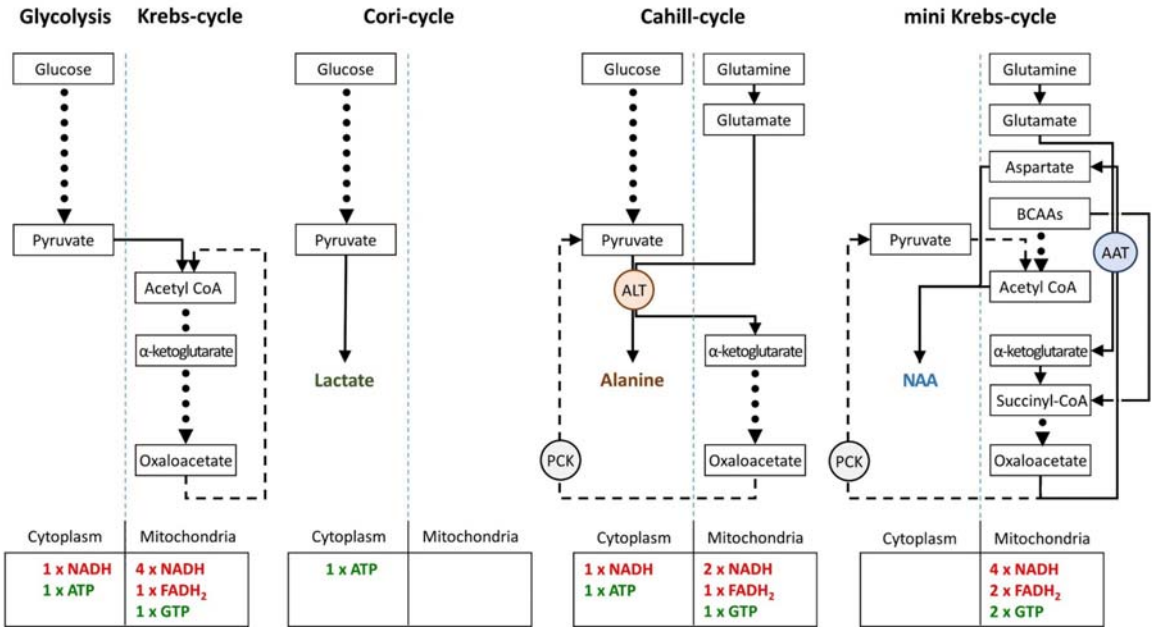


**Figure 8. Comparison of metabolic pathways and their energetic efficiencies.** Compared to the Cori-cycle, both Cahill- and mini-Krebs-cycles are highly efficient. Their key enzymes – alanine transaminase (ALT) and aspartate amino transferase (AAT), respectively – generate alanine and aspartate/N-acetylaspartate (NAA). Pyruvate carboxy kinase (PCK), either in cytoplasm or within mitochondria, may reconstitute pyruvate from oxalacetate. Note that energy output of each pathway was calculated based on input of pyruvate (three carbons) or glutamate/branched-chain-amin-acid/acetyl-CoA (three carbons).